SKY RESEARCH

Demonstration of Airborne Wide Area Assessment Technologies at Pueblo Precision Bombing Ranges, Colorado

– Hyperspectral Imaging –

Final Report

Project No. 200416

Prepared by
Sky Research, Inc.
445 Dead Indian Memorial Road
Ashland, OR 97520

Prepared for

Environmental Security Technology Certification Program

Submittal Date: September 27, 2007
Final v. 2.0

REPORT DOCUMENTATION PAGE

Form Approved
OMB No. 0704-0188

PLEASE DO NOT RETURN YOUR FORM TO THE ABOVE ORGANIZATION.

1. REPORT DATE *(DD-MM-YYYY)*	2. REPORT TYPE	3. DATES COVERED *(From - To)*
09-27-2007	Draft Final	May 2004 - December 2006

4. TITLE AND SUBTITLE

Demonstration of Airborne Wide Area Assessment Technologies at Pueblo Precision Bombing Ranges, Colorado - Hyperspectral Imaging

5a. CONTRACT NUMBER

W912HQ-05-C-0036

5b. GRANT NUMBER

5c. PROGRAM ELEMENT NUMBER

MM-0416

6. AUTHOR(S)

Dr. Jack Foley
Mr. Cameron Patterson

5d. PROJECT NUMBER

5e. TASK NUMBER

5f. WORK UNIT NUMBER

7. PERFORMING ORGANIZATION NAME(S) AND ADDRESS(ES)

Sky Research, Inc.
445 Dead Indian Memorial Dr.
Ashland, OR 97520

8. PERFORMING ORGANIZATION REPORT NUMBER

9. SPONSORING/MONITORING AGENCY NAME(S) AND ADDRESS(ES)

Environmental Security Technology Certification Program Office
901 North Stuart Street, Suite 303
Arlington, VA 22203-1821

10. SPONSOR/MONITOR'S ACRONYM(S)

ESTCP

11. SPONSOR/MONITOR'S REPORT NUMBER(S)

12. DISTRIBUTION/AVAILABILITY STATEMENT

Unlimited

13. SUPPLEMENTARY NOTES

14. ABSTRACT

Hyperspectral imaging (HSI) technology was demonstrated as part of ESTCP's Wide Area Assessment Pilot Program at the Pueblo Precision Bombing Range #2 in Colorado. HSI sensors were deployed from fixed-wing platforms as part of the high airborne data collection and analysis for WAA and augmented the analysis of other high airborne datasets collected at the demonstration site, including LiDAR, large scale orthophotography, and synthetic aperture radar (SAR). Although the HSI sensor by itself would not out-perform the LIDAR/Orthophotography sensor combination for general WAA site characterization, the demonstration showed that HSI imagery can be used for detecting and extracting large munitions-related features such as target aiming features, and can sometimes detect landscape disturbance patterns including surface disturbance features difficult to observe in other datasets. In addition, the HSI datasets were used in a multiple-sensor fusion process to perform false-alarm reduction through the generation of detailed vegetation models used to discriminate metal from vegetation in SAR surface object detections.

15. SUBJECT TERMS

Hyperspectral imaging, wide area assessment, vegetation modeling, multiple-sensor fusion

16. SECURITY CLASSIFICATION OF:			17. LIMITATION OF ABSTRACT	18. NUMBER OF PAGES	19a. NAME OF RESPONSIBLE PERSON
a. REPORT	b. ABSTRACT	c. THIS PAGE		40	Dr. John Foley
					19b. TELEPHONE NUMBER *(Include area code)* 978.458.9807

Reset

Standard Form 298 (Rev. 8/98)
Prescribed by ANSI Std. Z39.18

TABLE OF CONTENTS

LIST OF FIGURES

LIST OF TABLES

ACRONYMS

µm	micrometer
AGL	Above Ground Level
AP	Armor Piercing
ASR	Archive Search Report
BSQ	Band Sequential
BT3	Bomb Target #3
BT4	Bomb Target #4
cm	centimeter
COC	Certificate of Clearance
DEM	Digital Elevation Model
DERP	Defense Environmental Restoration Program
DoD	Department of Defense
DOI	Department of Interior
ESTCP	Environmental Security Technology Certification Program
FOV	Field of View
FUDS	Formerly Used Defense Site
GIS	Geographic Information Systems
GLT	Geographic Look-up Table
GP	General Purpose
GPS	Global Positioning System
HE	High Explosive
HSI	Hyperspectral Imaging
IFOV	Instantaneous Field of View
IMU	Inertial Measurement Unit
km	kilometer
LiDAR	Light Detection and Ranging
m	meter
MF	Matched Filter
mm	millimeter
MNF	Minimum Noise Fraction
MRA	Munitions Response Area
mrad	millirad
MRF	Munitions Related Feature
MRS	Munitions Response Site
NIR	Near Infrared
nm	nano meter
OB/OD	Open Burn/Open Detonation
PBR#2	Precision Bombing Range #2
PPI	Pixel Purity Index
RGB	Red, Green, Blue (true-color)
RMSE	Root Mean Squared Error

ROC	Receiver Operating Characteristics
SAR	Synthetic Aperture Radar
SimOrd	Simulated Ordnance
SNR	Signal to Noise Ratio
SWIR	Short-wave Infrared
UXO	Unexploded Ordnance
VIS	Visible
WAA	Wide Area Assessment

ACKNOWLEDGEMENTS

Demonstration of Airborne Wide Area Assessment Technologies at Pueblo Precision Bombing Ranges, Colorado, Hyperspectral Imaging documents the acquisition, processing, analysis, and interpretation of airborne remote sensing data for unexploded ordnance-related sites at the former Pueblo Precision Bombing Ranges. The work was performed by Sky Research, Inc. of Oregon, with Dr. John Foley serving as Principal Investigator for this project. Funding for this project was provided by the Environmental Security Technology Certification Program Office. This project offered the opportunity to examine advanced airborne methods as part of the Department of Defense's efforts to evaluate wide area assessment technologies for efficient characterization and investigation of large Department of Defense sites.

We wish to express our sincere appreciation to Dr. Jeffrey Marqusee, Dr. Anne Andrews, and Ms. Katherine Kaye of the ESTCP Office for providing support and funding for this project. In addition, we thank HyVista Corporation of Australia for their participation in the collection and processing of hyperspectral data at the site.

ABSTRACT

Wide Area Assessment (WAA) technologies and methodologies hold great promise for the efficient characterization of large sites relative to unexploded ordnance (UXO) contamination. WAA methodology provides a layered approach utilizing high airborne sensors, low airborne surveys, and ground-based surveys to continually refine the footprint of UXO contamination necessary for further decision making. To demonstrate the utility and applicability of these technologies, singly and in combination, the Environmental Security and Technology Certification Program (ESTCP) has undertaken a multi-site demonstration of WAA technologies through the creation of its Wide Area Assessment Pilot Program.

Hyperspectral imaging (HSI) technology was demonstrated as part of ESTCP's program at the Pueblo Precision Bombing Range #2 (PBR#2) in Colorado. HSI sensors were deployed from fixed-wing platforms as part of the high airborne data collection and analysis for WAA. HSI data collection augmented the analysis of other high airborne datasets collected at the demonstration site, including LiDAR, large scale orthophotography, and synthetic aperture radar (SAR).

Although the HSI sensor by itself would not out-perform the LIDAR/Orthophotography sensor combination for general WAA site characterization, and did not meet expected performance criteria in several areas, this demonstration showed that HSI imagery can be used for detecting and extracting large munitions-related features such as target aiming features, and can sometimes detect landscape disturbance patterns including surface disturbance features difficult to observe in other datasets. In addition, the HSI datasets were used in a multiple-sensor fusion process to perform false-alarm reduction through the generation of detailed vegetation models used to discriminate metal from vegetation in SAR surface object detections.

HSI may also be useful for the direct detection of metallic objects such as UXO and munitions scrap. The use of hyperspectral data to detect surface concentrations of metal materials depends on the size and spectral characteristics of the metal objects to be detected as well as the spectral characteristics of the background against which they must be detected. At the Pueblo PBR#2 site, background soils with abundant iron content made direct detection of surface metal concentrations using HSI problematic. This report provides a quantitative analysis of this phenomenological issue and provides recommendations regarding the spatial and spectral resolution requirements and detection phenomenology parameters necessary to make direct UXO materials detection with HSI useful in a WAA scenario.

For future WAA projects, HSI should be considered for inclusion in the multiple-sensor high airborne program if SAR is to be used for surface UXO detection, or if pre-WAA ground investigation indicates that munitions-related features related to soil chemistry or unique vegetation/disturbance factors can be best detected using the HSI sensor.

Airborne imaging spectrometers are undergoing continual improvements in resolution, quality, availability, and deployment costs. Therefore, it is worthwhile to consider their use for new WAA production deployments based on pre-deployment field studies and the munitions response site detection phenomenology unique to the subject site.

1. INTRODUCTION

1.1. Background

Unexploded ordnance (UXO) contamination is a high-priority problem for the Department of Defense (DoD). The DoD has estimated that approximately 10 million acres of potentially contaminated land may exist within approximately 1,400 DoD sites identified to date. Because many installations are very large, comprising tens of thousands of acres, efficient investigation methods are clearly needed to characterize these sites. In addition, it is estimated that only a percentage of the estimated 10 million acres is actually contaminated with UXO. Therefore, DoD has identified the need to utilize a technology or combination of technologies to accurately delineate the contaminated areas on each site to significantly reduce the actual area requiring further investigation and remediation. To investigate the use and applicability of these Wide Area Assessment (WAA) technologies for large scale site investigation of UXO sites, the Environmental Security and Technology Certification Program (ESTCP) designed a Wide Area Assessment Pilot Program. This program consists of demonstrations to validate the application of a number of recently developed and validated technologies as a comprehensive approach to Wide Area Assessment.

The use of WAA technologies can be described as a layered approach to site characterization that continuously refines geophysical site information. First, various sensors are deployed from fixed- or rotary-wing aircraft, referred to as "high-airborne" technologies. These sensors can include Light Detection and Ranging (LiDAR) sensors for measuring variation in surface elevation, large-scale orthorectified photography for visual identification of features of interest, hyperspectral imaging (HSI) for detection of surface reflectivity variations either across the entire visible portion of the spectrum or within narrow wavelength bands, and synthetic aperture radar (SAR) for detection of variation in reflectivity and polarization in the radar bands. All of these sensors are of appropriate design to detect anomalies that can be referred to as "munitions-related features (MRFs)," including target rings, craters, and possibly surface metal that can be associated with the presence of UXO.

Next, a helicopter-borne magnetometer array can be deployed over areas identified by the high airborne sensors for further investigation to detect subsurface ferrous metal directly. The magnetometer data can be analyzed to extract either (1) distributions of magnetic anomalies which can be used to locate and bound targets, aim points, and open burn/open detonation (OB/OD) sites; or (2) individual anomaly parameters (location, depth, rough size, etc.) that can be used in conjunction with target remediation to validate the results of the magnetometer survey. Last, ground surveys are conducted with the goal of defining target locations and bounds and also to validate previous results of high airborne and helicopter surveys.

This report details the demonstration of HSI technology at Pueblo Precision Bombing Range #2 (PBR#2) in Colorado as one technology in a suite of high airborne technologies within the larger context of a WAA demonstration at the Pueblo PBR#2 site. The HSI demonstration was

conducted in two phases; Phase I was initiated in May 2004 and Phase II in 2005. Additional high airborne data sets were also collected as part of the WAA demonstration, including LiDAR and orthophotography (Phases I and II) and SAR (Phase I).

1.2. Objectives of the Demonstration

The purpose of the WAA Pilot Program is to demonstrate and evaluate the use of technologies suitable for WAA of suspected munitions contaminated sites. The objective of the overall program is to demonstrate the effectiveness of a range of investigation technologies, used singly or together, in supporting decisions to be made concerning large range areas. In turn, the ability of these technologies to identify munitions response sites (MRSs), characterize site conditions for future work, and investigate areas outside of the MRSs in support of decision making is being evaluated.

As one WAA technology of several demonstrated at the site, the objectives of the HSI demonstration were as follows:

- Demonstrate the achievable geospatial accuracy and resolution of HSI datasets;
- Detect bombing target features and other large MRFs with analyst-mediated interpretive procedures;
- Detect surface concentrations of munitions-related metallic materials; and
- Contribute spectral information to a multiple-sensor vegetation model used to mitigate false-alarm metal detections in SAR data processing and modeling.

1.3. Regulatory Drivers

This site and the associated impact areas are classified by the United States Government as a Formerly Used Defense Site (FUDS) under the Defense Environmental Restoration Program (DERP).

1.4. Stakeholder/End-User Issues

ESTCP is managing the stakeholder issues as part of its WAA Pilot Program. ESTCP plans to use a process that will ensure that the information generated by the helicopter, water, and validation surveys is useful to a broad stakeholder community (e.g., technical project managers and Federal, State, and local governments, as well as other stakeholders).

2. TECHNOLOGY DESCRIPTION

2.1. Technology Development and Application

2.1.1. Sensor Description

The HSI system used in this demonstration was a HyMap operated by HyVista Corporation of Sydney, Australia. While a number of airborne imaging spectrometers exist and the technology is in active commercial use for a variety of geological and vegetation mapping efforts, the Hymap sensor offered the best available combination of spectral and spatial resolution, signal to noise ratio (SNR), and geospatial accuracy necessary to achieve the demonstration objectives. The HyMap is an airborne hyperspectral sensor that measures the electromagnetic spectrum from 0.45 micrometer (μm) to 2.5 μm in 126 separate but contiguous bands that have variable widths (from 15 nanometers [nm] in the visible wavelengths to 17 nm in the short-wave infrared [SWIR] wavelengths). HyMap records an image by using a rotating scan mirror which allows the image to build line by line as the aircraft flies forward. The reflected sunlight collected by the scan mirror is then dispersed into different wavelengths by four spectrometers in the system. The spectral and image information from the spectrometers is digitized and recorded on tape. The many contiguous bands of a hyperspectral imager produce complete spectral signatures associated with each recorded pixel (Figure 1) that allow for identification of materials rather than simple discrimination afforded by most space-based remote sensing instruments (e.g., Landsat) or airborne multi-spectral instruments.

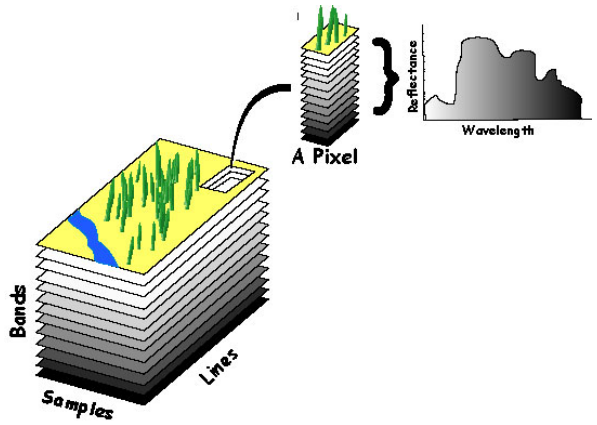

Figure 1. The general hyperspectral imaging concept; measurement of reflected electromagnetic radiation across many tens of contiguous bands where each pixel contains one complete spectral signature used to absolutely identify surface materials.

To minimize distortion induced in the image by aircraft pitch, roll and yaw motions, the HyMap is mounted in a gyro-stabilized platform. While the platform minimizes the effects of aircraft motion, small image distortions remain. These residual motions are monitored with a 3-axis gyro, 3-axis accelerometer system [inertial measurement unit (IMU)]. Dedicated geo-correction processing restores the full geo-location information and allows the creation of geographic

information system (GIS)-ready products. The HyMap system (Figure 2) operates in aircraft with standard aerial photo-ports and images with an angular width of 61.3 degrees (approximately 2.3 kilometers [km] at 2000 meters [m] above ground level [AGL]). Data were acquired for this study at spatial resolutions of 1.5 and 3 m/pixel. At the 1.5 m resolution, under-sampling that occurred in a small part of the imagery was offset by the improved spatial resolution for vegetation-related feature detection aspects of the application. Table 1 summarizes the general operational characteristics of the HyMap system.

Figure 2. The HyMap instrument mounted in a twin-engine light aircraft with gyro-stabilized mount and looking through a standard aerial photo port.

Table 1. HyMap Sensor Description

Sensor	HyMap
Platform	Light, twin-engine aircraft
Ground pixel size	2.5-10 m (optimal); 1.5 m minimum
Ground Speed	110-180 knots typical; slower for smaller pixel size
Altitude	2000-5000 m AGL typical; lower for smaller pixel size
IFOV (instantaneous field of view)	2.5 millirad (mrad)
FOV (field of view)	61.3°
Swath	1.8 km at 2.5 m IFOV; 2.3 km at 5 m IFOV
Accuracy	± 1-1.5 pixels (≥3m pixels)
Wavelengths	0.45 µm – 2.5 µm
SNR	>1000:1

2.1.2. Sensor Calibration

The HyMap sensor acquires reflected surface radiation which needs to be calibrated and corrected for atmospheric absorption to derive reflectance. Reflectance is then used for spectral signature analysis and comparison to spectral libraries of known materials. Using calibration parameters obtained in the laboratory, the initial digital numbers are converted to 'radiance at sensor' in mW/cm^2 *sr nm* radiance units. The atmospheric correction algorithm ATREM + EFFORT was applied to the data in order to convert 'radiance at sensor' into reflectance using information about the atmosphere, sun angle, geographic location, and time of survey.

2.1.3. Geo-positioning

No separate ground control was used during HyMap surveys. All spatial correction information was collected on-board the aircraft using a C-MIGITS II IMU, and geo-corrections were accomplished post-survey using the global positioning systems (GPS) information collected during the mission. An assessment of geo-location accuracy indicates that the basic accuracy is on the order of 1-1.5 pixels. This level of spatial accuracy was adequate for the large-target feature detections. However, geo-correction improvement was required for spectral sharpening of the high-resolution orthophoto and LiDAR datasets, as well as for generating a detailed fusion vegetation classification for SAR false-alarm mitigation. Geo-correction was accomplished using control tie-points derived from the orthophotography.

2.2. Previous Testing of the Technology

The HyMap HSI technology used for this demonstration has been in commercial and scientific use for geological resource mapping, environmental monitoring, agriculture and various research applications since 1999. In 2000, Sky Research used HSI technology to discriminate vegetation in SAR datasets at Former Lowry Bombing and Gunnery Range near Aurora, Colorado; however the Pueblo demonstration is the first attempted use of an HSI sensor to directly detect ferrous surface metal for UXO site characterization and the first successful use for detecting munitions target features not visible in conventional orthophotography or high-resolution topographic data.

2.3. Factors Affecting Cost and Performance

The principal factor affecting cost and performance of this relatively new technology is the availability of a suitable instrument. Although it was the best available instrument for the demonstration objectives, the limited availability of the HyMap sensor could be a limiting factor for more widespread use in UXO site characterization.

The spatial resolution and inherent geo-correction accuracy of the instrument limited the capability to directly detect small metal objects without extensive post-processing and fusion with high-resolution 3-band ortho-imagery to achieve the spatial resolution necessary to discriminate vegetation-related individual SAR targets. Therefore, the post-processing labor costs increase the overall cost of the technology use. However, improvements in spatial resolution and accuracy, improved spectral resolution, and SNR in airborne imaging spectrometers will reduce post-processing labor and thus decrease the cost of the technology's use for WAA efforts.

2.4. Advantages and Limitations of the Technology

Compared to competing technologies that may be applied for the purpose of WAA, the main advantage of HSI is in generating highly detailed IR + visible reflectance spectral data for individual geolocated pixels on the ground surface. Because these spectra are highly correlated with chemical composition, HSI data can be applied in three critical and unique ways:

(1) HSI spectra can directly signal the presence of exogenous surface objects and materials, including metallic munitions components and chemical salts from munitions compounds.
(2) Conversely, HSI spectra can be used to positively identify non-munitions-related features such as vegetation, which enables reducing the false-alarm rate from SAR data.
(3) Mapping based on filtered HSI spectra can reveal patterns of soil and vegetation disturbance caused by target construction, target usage, and/or munitions impact – patterns that often remain hidden on other datasets such as orthophotography.

The limitations of the technology currently relate to spatial and spectral resolution and geo-correction accuracy. Secondly, HSI datasets are large, requiring the IT infrastructure to manage, process and store the data. These limitations are expected to diminish as new or improved technologies are developed in response to the rapidly growing market for high-resolution geospatial data in a broad spectrum of applications domains, and as computing resources continue to expand in speed and power.

3. DEMONSTRATION DESIGN

3.1. Performance Objectives

The primary performance objectives relate to the attainment of resolution and coverage specifications for the basic HSI data collection (Table 2). In addition, secondary performance objectives relate to the contribution HSI datasets provide to the WAA process, including:

- Detect bombing target features and other large MRFs
- Detect surface concentrations of munitions-related metallic materials
- Contribute spectral information to a multiple-sensor vegetation model used to mitigate false alarm metal detections in the SAR data processing and modeling

These secondary objectives are provided in Table 3.

Table 2. Primary Performance Objectives

Type of Performance Objective	Primary Performance Criteria	Expected Performance (Metric)
Qualitative	Ease of use and efficiency of operations	Efficiency and ease of use meets design specifications
Quantitative	Geo-reference position accuracy	3 – 4.5m RMSE
	Spatial resolution	3m and 1.5m
	Spectral resolution	126 bands (0.45 μm – 2.5 μm)

In addition, there are secondary performance objectives that relate to the contributions that HSI datasets may potentially provide to the WAA process, including:

- Detecting bombing target features and other large MRFs;
- Detecting surface concentrations of munitions-related metallic materials; and
- Contributing spectral information to a multi-sensor vegetation model used to mitigate false-alarm metal detections in the SAR data processing and modeling.

Table 3. Secondary Performance Objectives

Type of Performance Objective	Secondary Performance Criteria	Expected Performance (Metric)
Quantitative	Pd: Surface Metal Objects > 1500gm	>0.80
	Pd: Target Features and other large MRFs	>0.90

3.2. Selected Test Site

The demonstration site consists of a total of 67,769 acres and is located approximately 20 miles south of La Junta, Colorado, in Otero County (Figure 3). The closest community is La Junta, a rural town with a population of about 7,637. The Phase I subset of the demonstration site comprised 6,710 acres centered on the Bomb Target 4 (BT4) area; the Phase II subset of the demonstration site included the Bomb Target 3 (BT3) area to the north, the suspected 75 millimeter (mm) Range, and BT4. The Phase II subset area covered approximately 3,044 acres, including overlap of the Phase I data collection area. See Figure 6 for Phase I and Phase II data collection area boundaries.

The site was chosen for its relative absence of post-military use disturbance and as being representative of large World War II bombing ranges across the western United States. Several known or suspected bombing/gunnery targets were included in the study area, as well as hypothesized areas of no contamination. The site was favored by state and federal regulatory and munitions management officials for inclusion in the WAA Pilot Program.

3.3. Test Site History/Characteristics

3.3.1. Test Site History

The munitions response area (MRA) was used by local populations for cattle grazing until the War Department assumed control of the lands to construct the Pueblo Precision Bombing and Pattern Gunnery Range #2 (1942 to 1946). During active operations the ranges were under the Western Flying Training Command, supporting Pueblo Army Air Field as part of the Second Air Force. A variety of activities took place in the 67,769-acre range that encompasses the Pueblo PBR #2. The training ranges consisted of a bombing camp with two runways and nine precision bombing targets, along with an air-to-ground pattern gunnery range. A map of the WAA Demonstration Area is shown in Figure 3 with the known and suspected targets indicated.

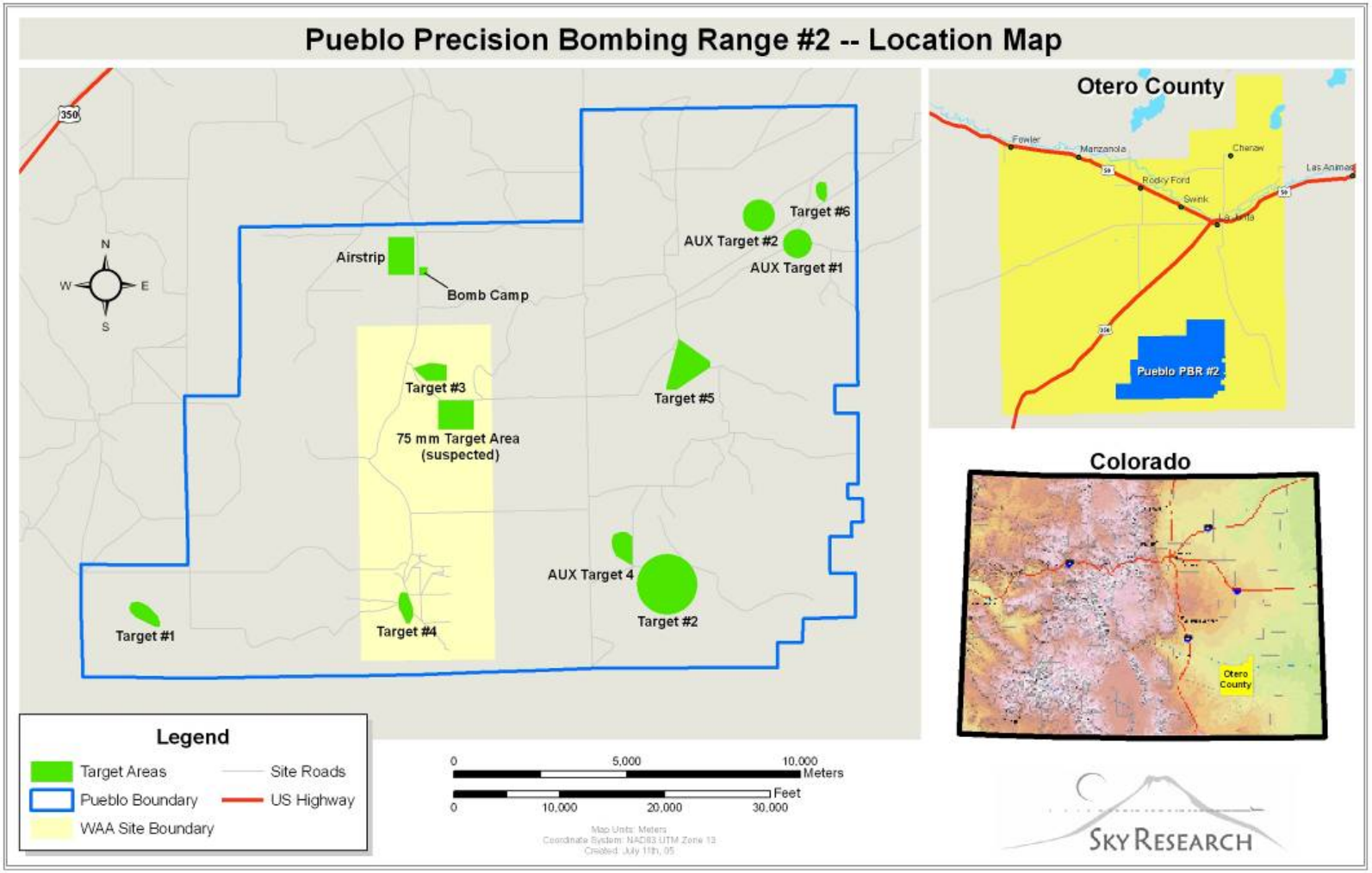

Figure 3. Pueblo PBR#2 entire WAA study area and vicinity map (source: Versar 2005).

In March 1943, E-1 sonic bomb scoring targets were installed at five of the Pueblo PBR #2 targets. In December 1944 crews also constructed a ship and a submarine target for the 471st Combat Crew Training School. The training documents indicate that the ranges were heavily used. During flight training, aviators used M-38A2 100-pound practice bombs as part of the May 1943 Second Air Force training requirement.. The training requirements (May 1943 Second Air Force) were First Phase 148 bombs, Second Phase 155, Third Phase 154. In January 1944, crews completed 672 high-altitude bombing releases during training. In March 1944, the 491st Bomb Group completed 1,449 high-altitude bombing releases. In 1944, Chinese B-25 Mitchell Bomber students practiced firing 75 mm cannons using the M72 shot, armor-piercing projectile. From 28 August to 1 October 1945, the intended training also included rocket firing, ground gunnery (50 caliber), aerial gunnery, and dive bombing, with each pilot firing 30 rockets and dropping 20 bombs

In August 1946, Tibbits Contractors Inc. conducted a surface clearance in the MRA and issued a Certificate of Clearance (COC). It is not known how much of the range was cleared under this contract, nor is the location of the clearance indicated. However, it is probably reasonable to assume that the clearance was done on the established bombing targets, probably including those in the study area (Bomb Targets 3 and 4). During the surface-only clearance, incendiary bombs (4-pound AN-M50A1 magnesium-type incendiary bomb), M38A2 practice bombs, and AN-M30 general-purpose (GP) high explosive bombs were identified. The COC stated that the land was surface cleared and free from explosives for the land use of cattle grazing. Also in 1946, the Department of the Interior (DOI) cleared a 1,400-acre portion of the MRA, which again was not identified, except that the Archive Search Report (ASR) noted that the clearance results indicated it was not part of the bombing targets. A COC was not issued for the DOI effort.

The following are munitions that have been found on Pueblo PBR #2 MRA and were included in the ASR:

- Bomb, GP, 100-pound, AN-M30 and AN-M30-A1
- Bomb, Practice, 100-pound, M38A2
- Bomb, Practice, 100-pound, Mk 15 Mod 3
- Bomb, Incendiary, 4-pound, AN-M50A1
- Shot, Armor-Piercing (AP), M72 (75 mm)
- Small Arms Ammunition, Caliber 50

The majority of the site is now owned and managed by the U.S. Forest Service as a part of the Comanche National Grasslands. However, some portions of the site are private or State-owned and some parcels in the middle of the study area are privately owned. The primary land use is cattle grazing. The general recreational use of the site is very broad and encompasses hiking, camping, and all-terrain vehicle use.

3.3.2. Test Site Characteristics

The site is located in the Colorado Piedmont section of the Great Plains physiographic province. Geological formations consist of Carlile Shale, Codell Sandstone, Greenhorn Limestone, and the Graneros Shale. The majority of the soils on site consist of light brownish-gray silty sandy clay. These soils have a moderate intake rate, medium to slow surface runoff, and moderate permeability. The erosion hazard is moderate to high on the steeper sloping areas of the site.

The terrain within the BT4 survey area consists of gently rolling plains interspersed with steeper drainages. There is greater terrain variability across the entire Pueblo PBR#2 site beyond the BT4 data collection area. Figure 4 illustrates a hillshade representation of the LiDAR terrain data within the BT4 data collection area.

Due to the relatively dry climate, vegetation on the site is characterized by prairie grasses and succulent, drought-resistant plants such as yucca, cholla and prickly pear cacti, juniper and piñyon pine trees, as well as other species of woody or succulent vegetation (Figure 5). At the time the site was flown, herbaceous vegetation was dry / senescent due to the late season, and optimal conditions probably existed for discriminating various vegetation types using spectral reflectance information.

3.4. Present Operations

As described above, a COC was issued after a surface clearance in 1946, presumably on the established bombing targets; also that year, the DOI cleared a 1,400-acre portion of the MRA, presumably in areas not identified as part of the bombing targets. No further remediation activities are known to have occurred within the MRA since then.

3.5. Pre-Demonstration Testing and Analysis

The basic HSI data collection technology used has been well established by HyVista. Prior to instrument deployment in the current project, specifications and sample datasets for this individual instrument were examined and compared with HSI data collected with other instruments for previous Sky Research projects.

3.6. Testing and Evaluation Plan

3.6.1. Demonstration Set-Up and Start-Up

Sky Research deployed the HSI sensor on a DHC-6/300 Twin Otter platform, together with sensor operator, pilot, copilot, and two-person ground support team to operate two GPS base stations and collect calibration panel spectra prior to each data collection. HyVista Corporation was subcontracted to supply the sensor operator and perform primary processing and to produce the geographic lookup table used to ortho-correct the image datasets of the classification results.

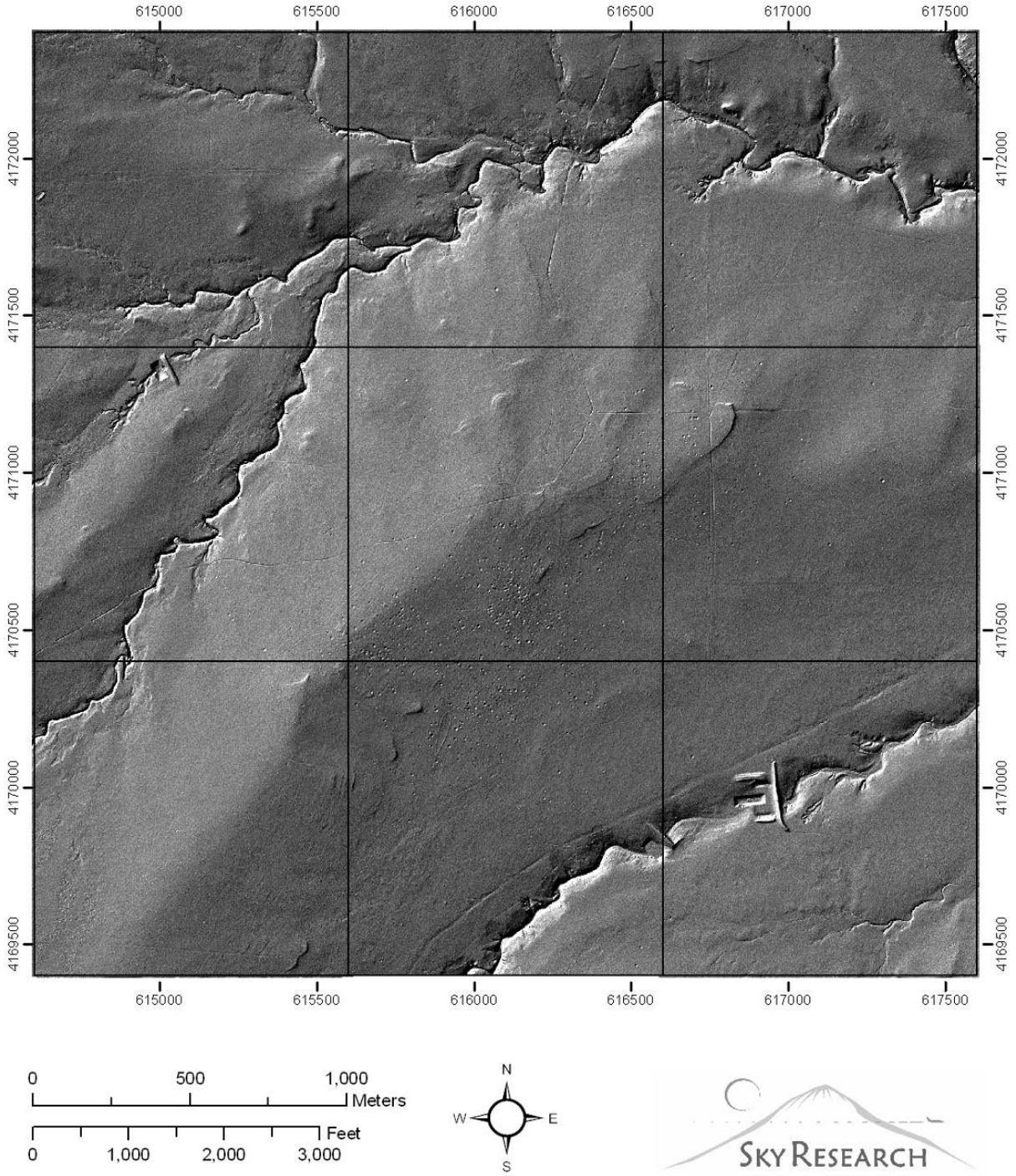

Figure 4. LiDAR hillshade imagery in the BT4 area.

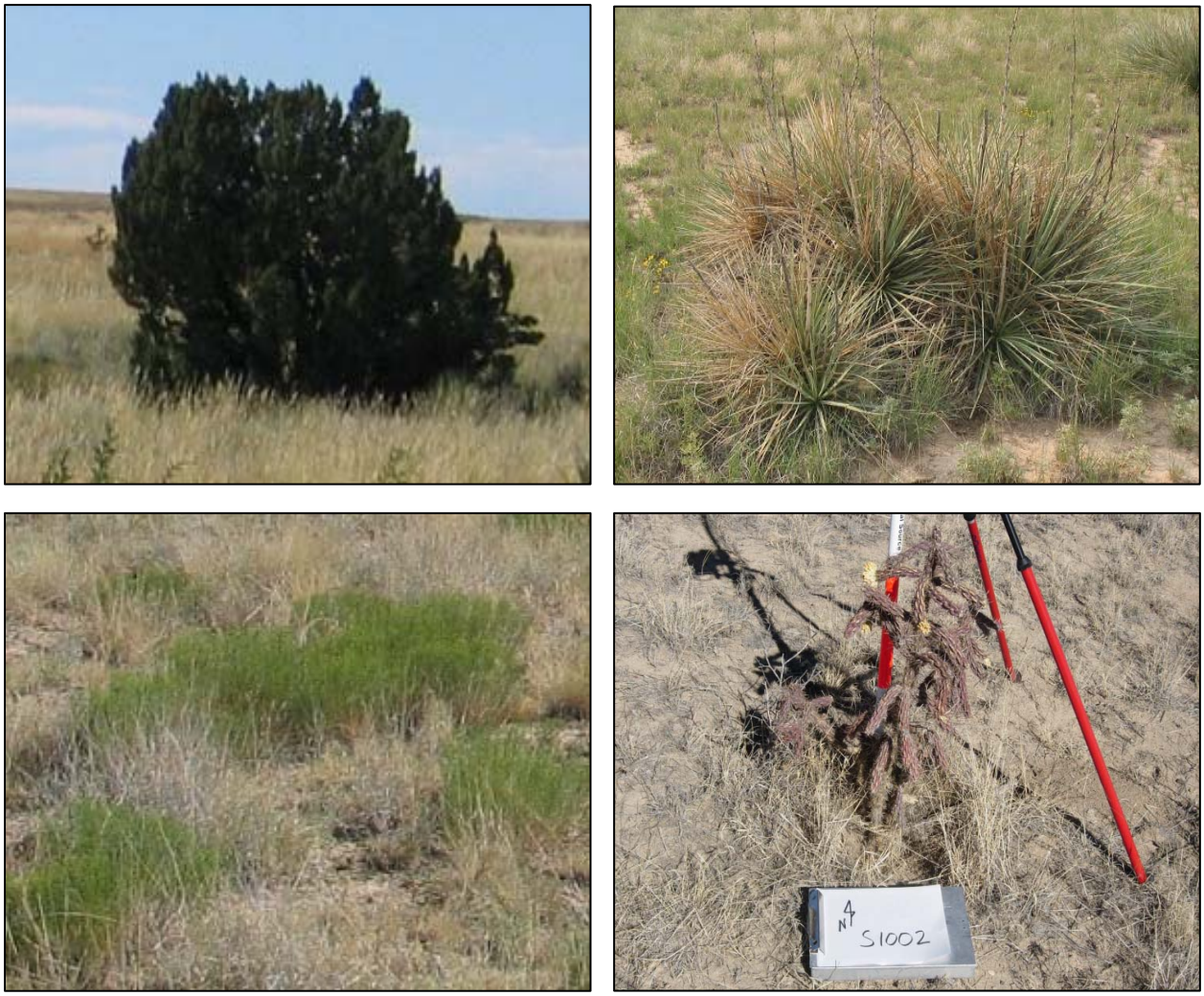

Figure 5. Typical vegetation found at the study area including juniper (upper left), yucca (upper right), various perennial forbs (lower left) and perennial bunch grasses and cholla (lower right).

3.6.2. Period of Operation

Phase I data collection occurred at Pueblo PBR#2 on September 17, 2004, covering approximately 6,710 acres. Data processing and analysis of Phase I data was conducted in 2004 and 2005, and vegetation mapping conducted in 2006 for SAR false alarm reduction. Phase II data collection occurred on August 30, 2005, covering a total of approximately 9,628 acres, 3,044 acres of which overlapped the Phase I data collection area. Data processing and analysis of the Phase II data was conducted in 2005 and 2006.

3.6.3. Area Characterized

A total of 10 Phase I image strips were collected covering the site with orthogonal swaths at both 3 m (4 strips) and 1.5 m (6 strips) resolutions. A total of 11 Phase II flight strips were collected at 1.5 m cell resolution. See Figure 6 for Phase I and Phase II data collection area boundaries.

3.6.4. Operating Parameters of the Technology

For Phase I data collection, image strips were collected covering the site with orthogonal swaths at both 3 m (4 strips) and 1.5 m (6 strips) resolutions. For the 3 m resolution data collection, the flight speed was about 100 knots at a flight altitude of about 1200 m. For the 1.5 m resolution, the sensor was deployed in an "under-sampling" mode where the integration rate was not adequate to keep up with the ground coverage rate. Data acquisition for 1.5 m resolution required flying at a lower flight speed (82 knots) and lower altitude (600 m AGL) than for the 3 m resolution data collection.

For Phase II data collection, a total of 11 flight strips were collected, all at 1.5 m cell resolution. As with the Phase I data collection at the 1.5 m resolution, the flight speed was 82 knots and the altitude was 600 m AGL.

3.6.5. Demobilization

Demobilization consisted of the aircraft, sensor, and flight and survey crews returning to their base of operations.

3.7. Analytical Methods

3.7.1. HSI Pre-Processing

Pre-processing conducted by HyVista data analysts consisted of processing the IMU and GPS flight positioning data and computing radiance images from raw sensor data. Atmospheric correction using the ATREM+EFFORT algorithm was applied to generate reflectance imagery. A final calibration of the reflectance data was performed to compensate for sensor characteristics affecting the overlap region of the component visible (VIS)/near infrared (NIR) – NIR2 spectrometers.

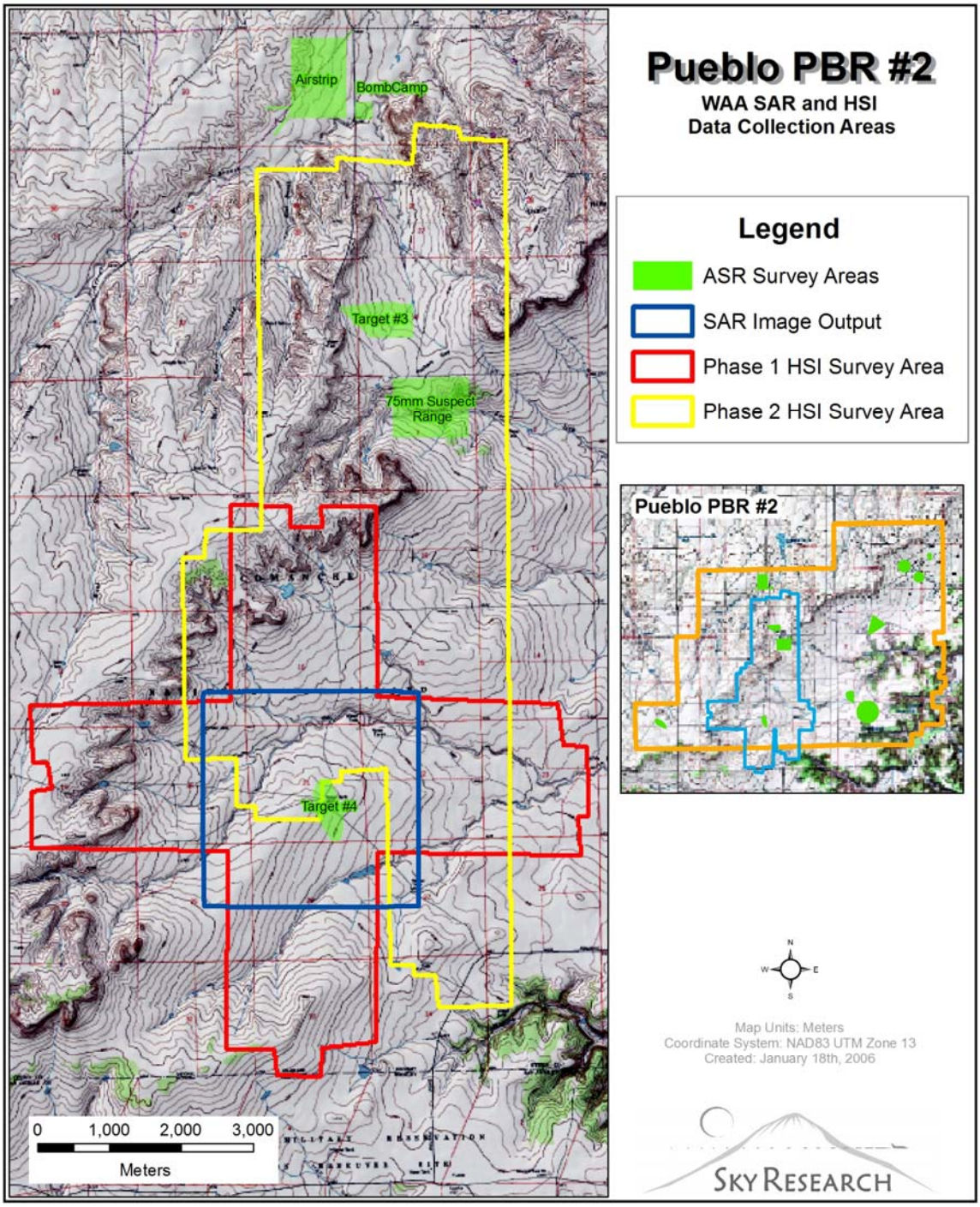

Figure 6. Phase I and Phase II HSI survey boundaries at Pueblo PBR#2.

3.7.2. HSI Processing

The following software packages were used for processing the HSI data:

- HyVista and ENVI software
- Image ortho-correction (HyVista incorporating LiDAR terrain data)
- Radiometric and atmospheric corrections (ENVI)
- Minimum Noise Fraction Processing (ENVI)
- Mixture Tuned Matched Filter/Spectral Unmixing (ENVI)
- Foreground-Background Analysis (FBA-IDL)
- Advanced Signal Processing Algorithms (Matlab/IDL)Advanced Signal Processing Algorithms (Matlab/IDL)

3.7.3. Calibration Analysis

Spectral image analysis was conducted using the reflectance imagery and field observations to determine the ability of the HSI datasets to map important vegetation classes and to detect and map surface metal objects. A set of spectral analyses was completed on a subset of the 1.5 m spatial resolution data centered on a target feature located at 615888E 4170196N (UTM 13, WGS84); see Figure 7. This target feature consists of a cleared and bermed region that mimics the shape of a naval vessel (approximately 150 m x 30 m in size). Analysis and interpretation was focused on determining the capability to identify and map important vegetation types and discriminate them from other image materials (rocks, soil, manmade, etc.), and to detect UXO either directly or by proxy.

Additional calibration analysis integrated field spectroscopy and ground-verification studies of the previously developed target maps. Two days were spent in the field (in November, 2004) with an ASD FieldSpecPro field spectroradiometer, where the goals were 1) to create a spectral library of dominant scene materials of interest; 2) field-check the target maps generated from the previous spectral analysis; and 3) generate field spectral training regions of interest to refine previous spectral mapping for UXO-related surface metal detection.

The initial analysis began with choosing four test-sites within each endmember class of Figure 8 to be field-checked using the field spectroradiometer. Each site was located using a portable Garmin 12x personal GPS (accuracies: 1 – 5 m). Spectral measurements were an average of 10 separate spectral measurements from a height of approximately 0.5 m above ground level. Iron oxide was successfully mapped at all 14 test-sites within each endmember class; however the overall UXO detection accuracy rate was only 64% (finding UXO where the pink pixels from Figure 8 were located). The error of commission (mapping UXO when there weren't any) was 38% and the error of omission (mapping no UXO when there were UXO) was 33%. The accuracy rate is high enough to suggest that there is merit in this hyperspectral-based mapping approach, but the error level suggests problems. Possible problems include the low sampling number (not statistically significant considering the size of the study-area), spatial accuracy between the HyMap geo-correction and the field GPS, and insufficiencies in the spectral techniques used.

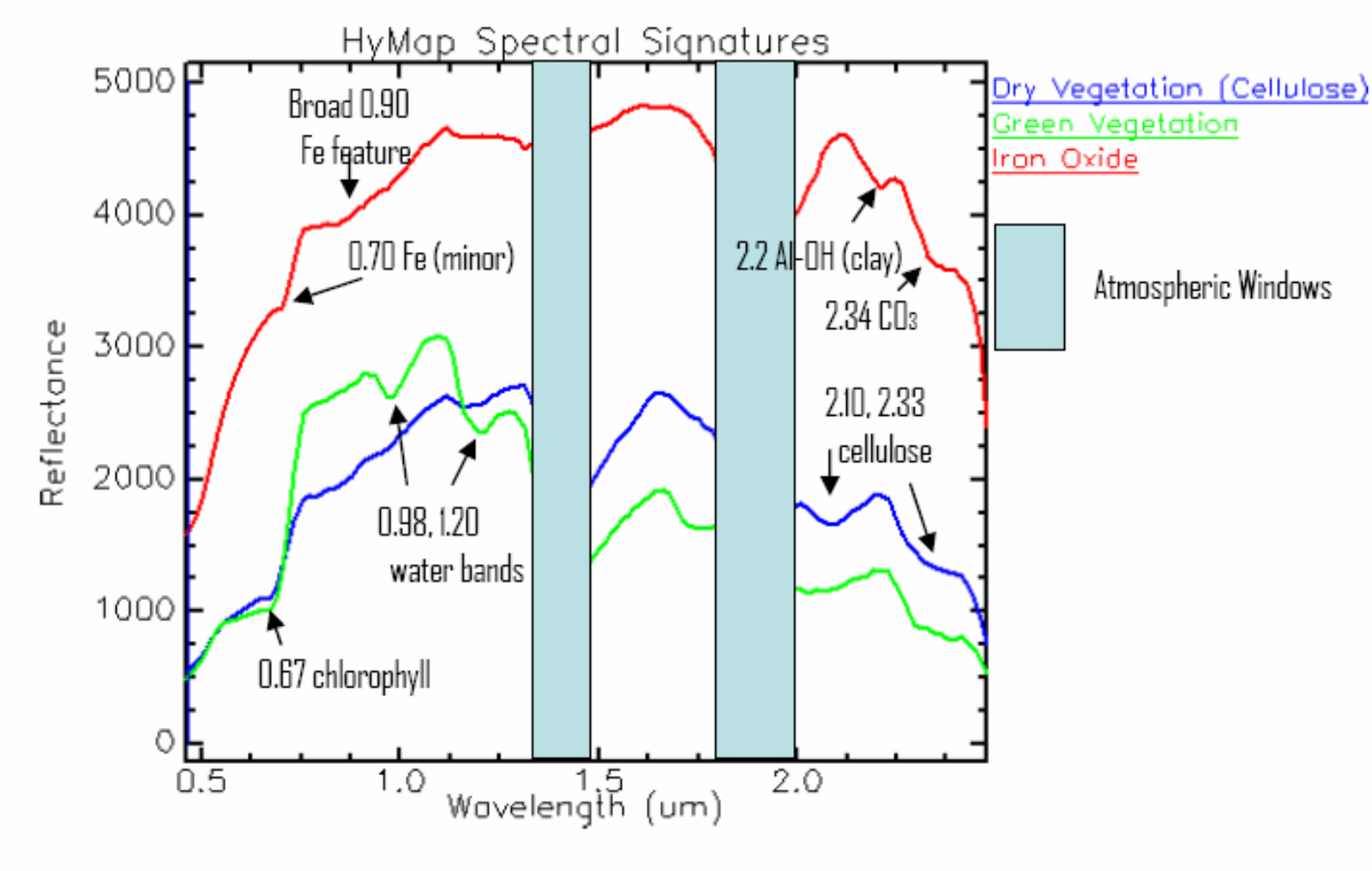

Figure 7. HyMap spectral signatures (126 bands) for three material groups of interest: dry vegetation, green vegetation and iron oxide. Important absorption features indicated.

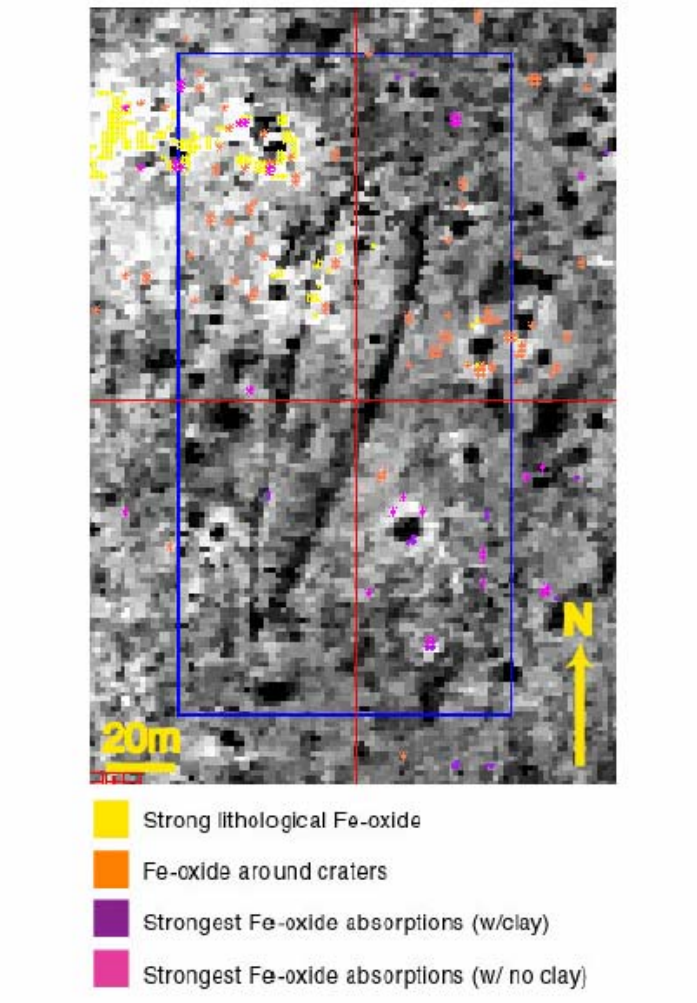

Figure 8. Iron-oxide mapping results of the Battleship study site. Background image is channel 109 (2.2μm) of HyMap.

The second analysis focused on quantifying what the materials of interest (especially UXO) looked like at high spatial and spectral resolution in order to better know what to look for at the lower spatial and spectral resolutions of airborne spectroscopy. Two important libraries were derived from this study including a vegetation library and a bomb material library (Figure 9).

Analysis of the spectral signatures of the five major plants in the study area reveals that each one is sufficiently distinct that plants can be identified within field spectra as well as imagery. Some spectrum variability results from seasonality, water content, and site factors for individual plant specimens, but if these factors are tracked in the metadata, then vegetation should be usable as a guide and discriminator.

Figure 9 shows analysis of the bomb spectra Spectral measurements made of intact bomb fragments (i.e., the measurement field of view [FOV] was entirely bomb fragment with no background soil included) revealed that there is a strong iron- oxide absorption in the NIR. This ~0.9 μm absorption for rusting metal is shifted slightly longward suggesting more weathering which is consistent with identification as goethite oxide absorption in the NIR. This ~0.9 μm absorption for rusting metal is shifted slightly longward suggesting more weathering which is consistent with identification as goethite.

The lithologic jarosite is shifted shortward in the 0.9 μm range meaning bomb fragments are goethitic in nature. The metal fragments also lack any clay or carbonate absorptions. Notice that the red signature labeled 'bomb spatter' does have some slight clay and carbonate absorptions due to the fact that the spectrum was taken of a multi-piece bomb spatter with soil showing through into the ASD FOV rather than of one intact fragment. The spectra also reveal an unknown phenomenon that appears to be associated with rusting metal. Signatures of bomb fragments have a marked negative slope in the SWIR 1 while the jarosite and the bomb spatter have positive slopes. This is very likely due to the weak Al-OH absorptions observed in the SWIR 1. Again, the rusted metal should not have any appreciable Al-OH. This bomb spectral library allows better spectral-based mapping for aged bomb fragments within hyperspectral datasets (by isolating those spectral regions with the strongest discriminatory capacity) as well as giving a basis for bomb mapping at other sites in the future.

3.7.4. Vegetation Analysis

The mapping and discrimination strategy for vegetation was simple: leverage the time of year (late September) to produce simple but robust maps of both dry/dead vegetation (via cellulose detection and tracking) and green vegetation (via tracking chlorophyll and leaf water). Spectral features indicative of biochemicals and physiological state are easily measured with a full-range spectrometer. The iron-oxide, water, and chlorophyll absorptions are tracked in the visible and near-infrared regions while the hydroxides and sulfates of minerals and the cellulose of vegetation are tracked in the SWIR region.

Vegetation classifications were generated using image extracted endmembers that were isolated using the "standard" data reduction techniques within the ENVI software. The algorithms are designed to find purest endmembers via spatial and spectral reductions. These endmembers are then used in a classification scheme to map the distribution of each extracted endmember. The results shown in Figure 10 demonstrate the ability to easily discriminate between vegetation and iron oxides. It also demonstrates the ability to differentiate between vigorous green vegetation and dead or dying vegetation.

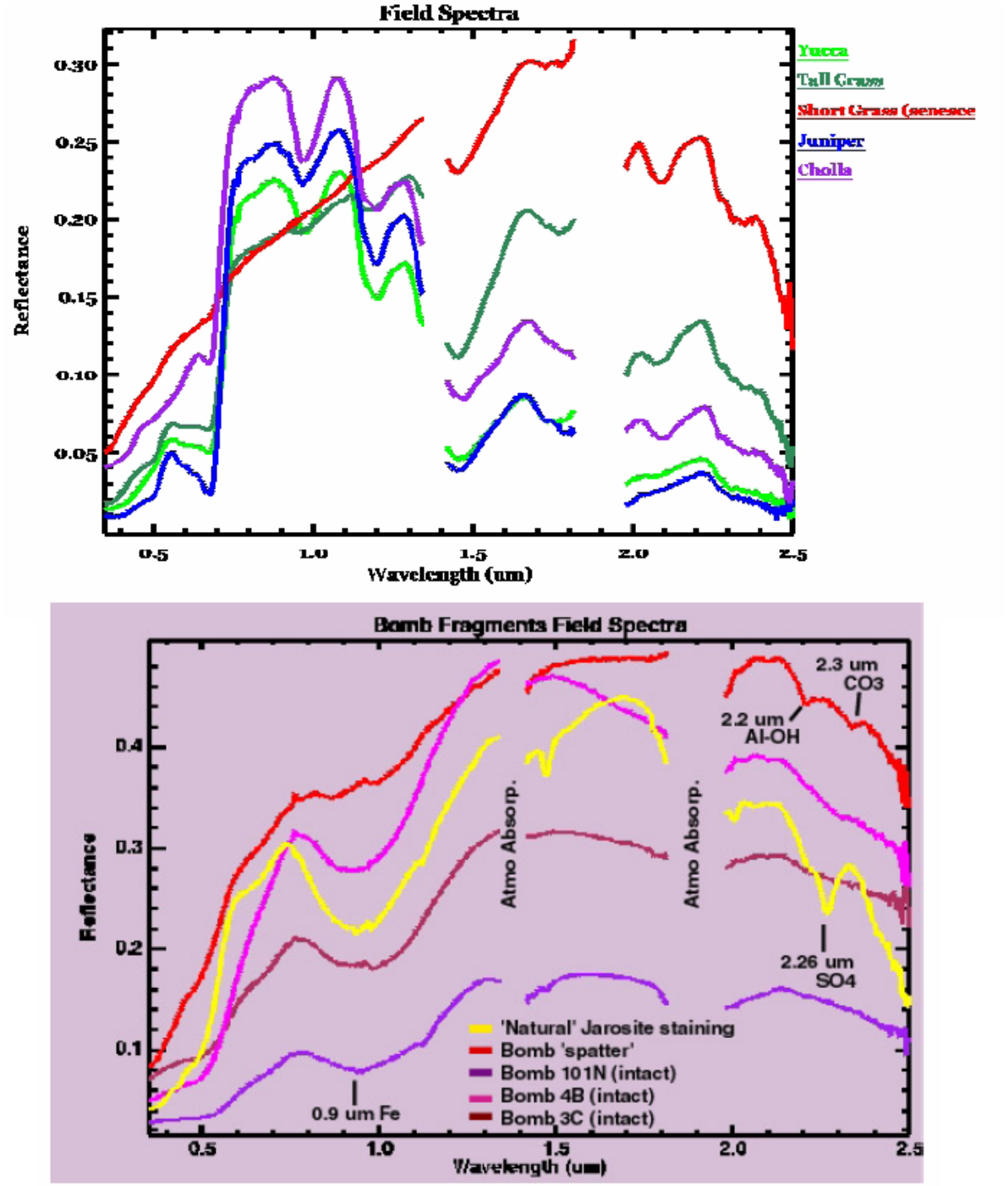

Figure 9. Top: Spectral plot showing field spectral measurements of various types of vegetation within the Battleship study area; all measured with the ASD. Each single spectrum represents an average of 10 spectral measurements. Bottom: Plot showing field spectral measurements of various metal bomb fragments in the same Battleship study area. A natural jarosite signature is included for reference.

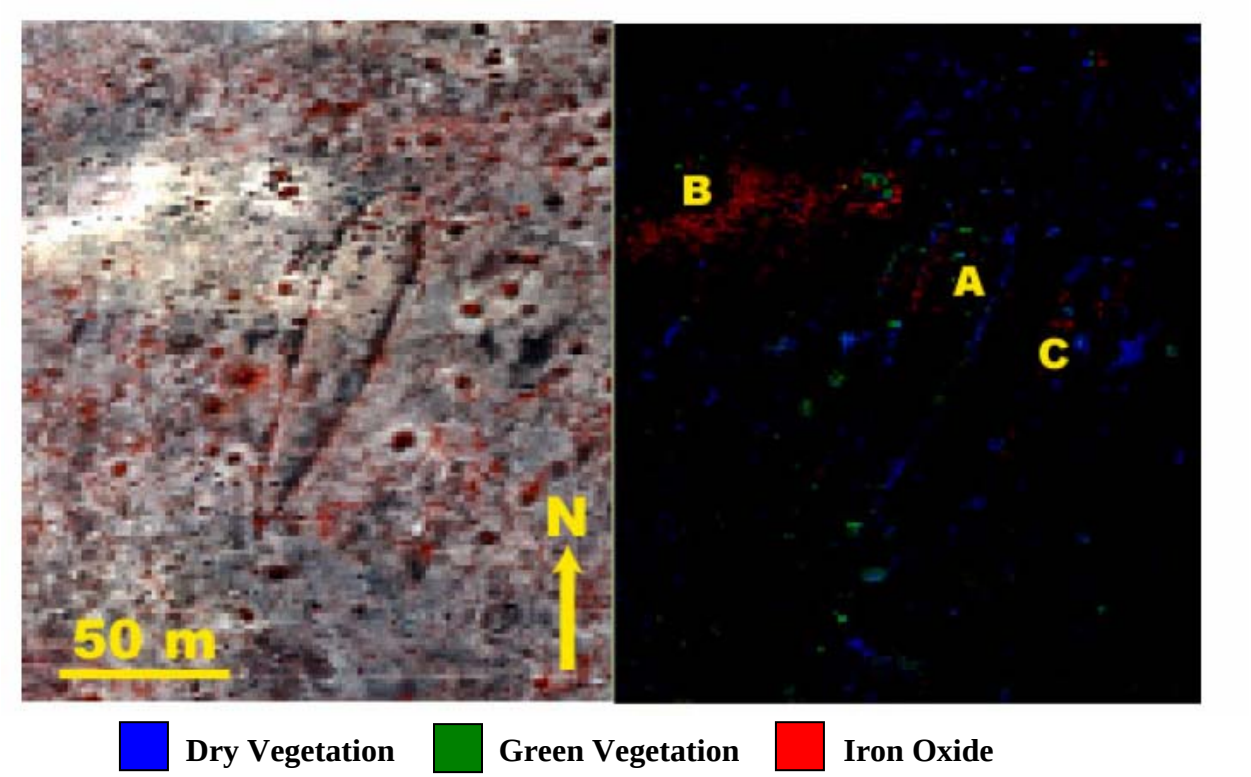

Figure 10. Left: Color-infrared HyMap image-subset ("battleship study site") centered on mock battleship where primary image analysis was completed. Right: Broad material classification delineating vegetation from iron oxides

Given an instrument that samples the entire VIS/NIR/SWIR spectral range such as HyMap, the discrimination of vegetation from minerals (including iron oxides) is relatively straightforward. This mapping strategy uses a broader spectrum rather than the VIS/NIR spectrum used in many satellite and photography studies. The SWIR is a key resource for vegetation mapping and discrimination. The reflectance of cellulose in the SWIR clearly distinguishes vegetation from iron oxides even if the spectral signatures are inconclusive in the visible and NIR wavelengths.

3.7.5. Surface Metal Analysis

The detection of metal associated with UXO was more difficult. The 1.5 m and 3 m image resolutions are too large for visual identification of individual UXO targets, so identification rests on target spectroscopy. Because of the typically long multi-decade *in situ* residence times, we relied on detecting the weathering products of aged UXO which are primarily iron oxides such as hematite, goethite, and limonite. Unfortunately, the natural environment also produces significant quantities of iron oxides and other oxides such as aluminum oxides and zinc oxides.

Therefore, the discrimination challenge became one of differentiating lithological iron oxide from iron oxides forming *in situ* on surface or shallow sub-surface metal.

The detection strategy entailed classifying the HyMap data for different iron oxide spectral endmembers (i.e., materials) that have measurable, consistent spectral features that imply a certain provenance and genesis. To distinguish natural forming iron oxides from iron oxides forming on anthropogenic materials such as UXO, we isolated the spectral signatures of these iron oxide endmembers and developed wide-area maps of their distributions with the intent to extract, isolate, and positively correlate a specific endmember with iron oxide minerals forming on and around surface UXO. Field verification and field spectral data improved these discriminations and identifications.

Initial 'spectral browsing' was completed via a principal components-based algorithm in ENVI [(MNF) Minimum Noise Fraction). This principal components-like algorithm allows analysis of the spectral variability within a scene and a preliminary identification of the types of material whose relative proportions are extractable from the dataset. This preliminary identification serves as a data familiarity and visualization tool as well as a source of endmember determination. Initially, a MNF analysis was completed over a study area spatial subset slightly larger than just the battleship study site shown in Figure 10. This provided familiarity with the overall spectral variability within the imagery and helped guide secondary processing.

The results of the MNF-based processing revealed a geobotanical relationship in which the co-occurrence of low-density short grass and high aluminum hydroxide / carbonate (Al-OH/$CO_{3)}$ soil appears to indicate the presence of berms associated with mock-battleship targets. This relationship was confirmed in the field. Within the study area, two additional battleship targets were identified in this manner that were not readily identifiable in the aerial photography or LiDAR images. These results supported the use of MNF-based data visualization and large-feature extraction across the entire study area.

Secondary processing focused on mapping, within ENVI, the endmembers statistically extracted from imagery. Spectral features in both the VIS/NIR and SWIR were used to isolate and identify dominant iron oxides via the MNF work and from subsequent pixel-purity index [PPI] work that isolates pixels containing the purest spectral representations of dominant scene materials. These iron oxide spectra were then used in directed spectral mapping algorithms; principally the Matched Filter (MF). The best MF iron-oxide mapping results are shown in Figure 8. All of the colored pixels contain iron oxide as a dominant surface component. While the yellow pixels are spectrally indicative of *in situ* lithological iron oxide and the orange pixels correspond to more highly weathered iron oxides, the purple and pink colored pixels appear as spectrally closest to iron oxide of a rusting metal origin. Theoretically the rusting metal should lack the clay minerals present in a standard rock-weathering profile and hence the final class of iron oxides containing little to no clay spectral features (colored in pink) should represent rusting metal; i.e., a proxy for UXO.

Though the actual identification of iron oxides was readily achieved, the determination of provenance and genesis of the oxides was challenging. The highly oxidized background

lithology of the study site, coupled with the small size of the targets, make the results of the image mapping inconclusive. As far as is known, iron oxide that forms within and on sedimentary/volcanic/igneous rocks looks spectroscopically the same as iron oxides forming on metals (at a pixel-scale). The suggestion that pixels over rusting metal may lack accompanying clay and carbonate absorptions was therefore field-tested.

3.7.6. Secondary Processing

Large Feature Extraction

To prepare HSI data to assist with gross feature extraction, ENVI MNF transformations were run on all 1.5 m resolution flightstrips, converting the 126-band reflectance data to reduced band-sets of 20 eigenbands. These MNF images were then geo-corrected using the geographic look-up tables (GLT), and converted to band sequential (BSQ) raster format for use in the ArcGIS visualization and feature extraction environment. Band combinations were mapped to the red-green-blue (RGB) image rendering channels after determining which bands and band combinations provided the best feature visualization for detecting known target features. The entire site was then systematically reviewed using single bands and band combinations, in conjunction with other imagery derived from LiDAR and orthophotography datasets. The Phase I and Phase II datasets were analyzed separately using the same basic procedures. In the Phase I area one ship target was extracted that was not visible in the other sensor data and one ship target that was partially visible in the other data was fully delineated. All other delineated large target features, both in Phase I and in Phase II, were confirmed by the HSI data.

Figure 11 illustrates the capabilities of the visualization environment used to review the imagery and extract detected large features. Both images are portions of HSI Flightstrip 5, which was transformed from 126 spectral bands into 20 MNF bands as described above. Image “A” shows the primary detection ship target as a false-color image that maps MNF bands 3, 4, and 1 into the RGB rendering channels. Image “B” shows a different ship target in a gray-scale rendering of MNF channel 9.

Because large feature extraction from these image datasets combines analyst image interpretation with automated processing algorithms such as hillshade computations, color stretches, and processing filters, confirming sensors play an important role. Figure 12 illustrates this by showing image chips for the BT4 target circle from HSI MNF Band 4, orthophotography with a normal stretch, and the LiDAR surface digital elevation model (DEM) hillshade. Although the target circle is visible to the analyst in all three datasets, different parts of the feature are visible in different datasets, increasing the accuracy of the extraction.

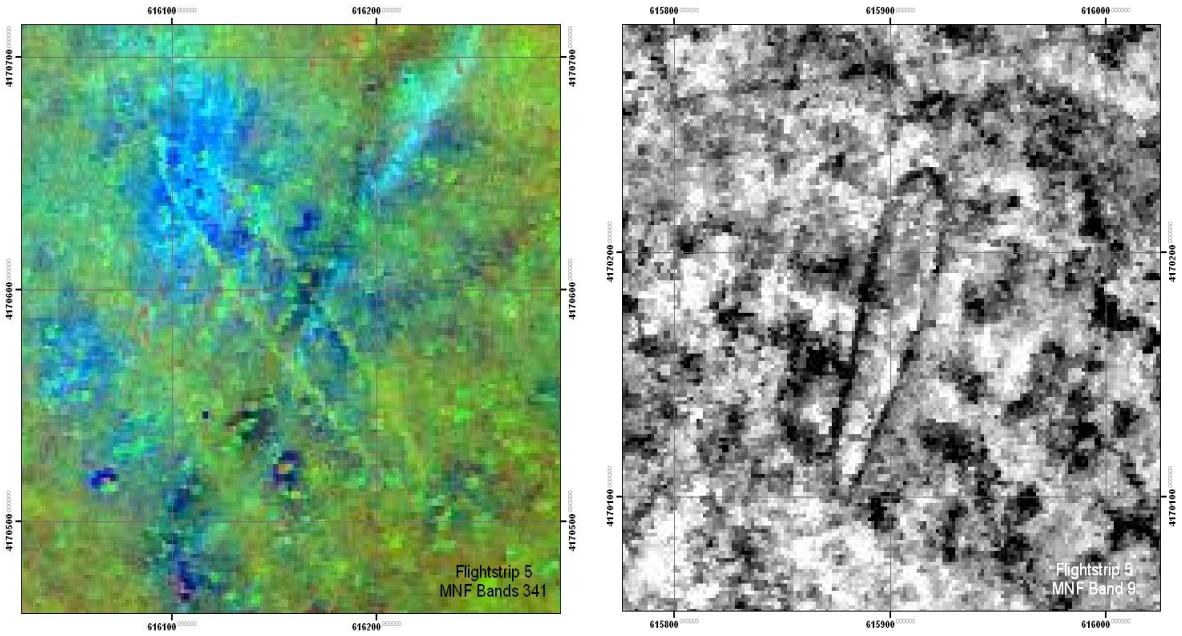

Figure 11. Ship targets near BT4 observed in HSI imagery.

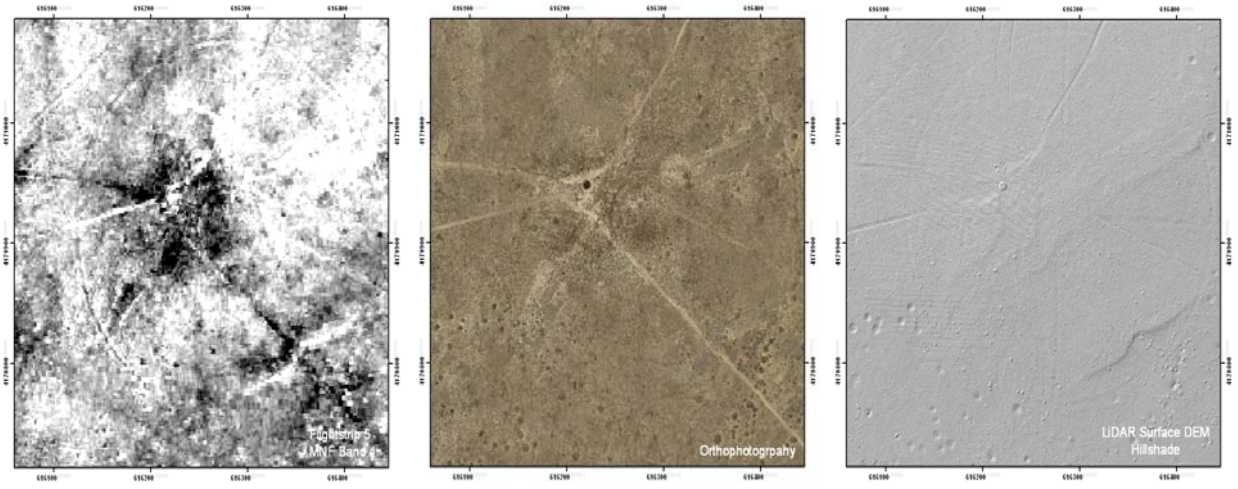

Figure 12. Left: Target circle at BT4 shown in imagery from HSI MNF Band 4. Center: orthophotography image. Right: LiDAR surface DEM hillshade.

Vegetation Modeling

Vegetation modeling using HSI data in conjunction with LiDAR and orthophotography data was performed for the SAR analysis extent in the Phase I area. The focus of this modeling was to generate feature detections for specific vegetation types that cause false alarm detections in the SAR imagery.

Vegetation modeling was designed to determine the spatial locations of the most abundant class of SAR scatterers present on the study area landscape: succulent and woody vegetation. The dielectric properties of water in live wood of trees and in the succulent stems and leaves of cactus and yucca are responsible for the majority of false-alarm SAR detections. Models of the spatial distribution of these plants objects were used to discriminate vegetation-caused SAR detections from those caused by metallic objects.

To generate a model of vegetation scatterers on the site sufficient to discriminate individual SAR targets, the spatial accuracy and resolution of the basic HSI dataset needed to be improved from the HyVista-delivered GLT specifications of about 5-12 m root mean square error (RMSE) horizontal radial error to an accuracy of less than one pixel. This was accomplished by registering the GLT-geo-corrected HyMAP data to the high-resolution (14 centimeter [cm]) orthophotography which had been determined to have a radial horizontal accuracy of better than 10 cm RMSE. The ENVI-IDL image registration tools were used to register the 1.5 m HSI data, clipped to 1 km^2 processing tile extents, with a residual horizontal RMSE of less than 0.5 m.

The HSI data were then combined with the 14 cm orthophoto data to compute high resolution vegetation indices that were able to discriminate individual vegetation objects such as yucca and cactus plants. The following steps were used to create the vegetation indices.

- 14 cm RGB orthophoto data were resampled to 25 cm pixels to match the SAR image resolution.
- The 126-band HSI data were fused with the 25 cm RED orthophoto band using a Principal Components spectral sharpening algorithm (Welch and Ahlers 1987) to generate 126-band spectral data at 0.25 m resolution.
- A broadband normalized difference vegetation index was computed from the high resolution spectral data using (RED-NIR) / (RED + NIR) to provide a robust detection of canopy chlorophyll content (Sellers 1985) strongly correlating with the green yucca, cactus, juniper, and other SAR-responsive vegetation species on the site.
- Canopy water content indices were computed corresponding to spectral water absorption features at 970 nanometers (nm) and 1200 nm to generate high-resolution measures of vegetation water content, which is highly correlated with SAR signal response. The two canopy water content indices used were based on the band ratios 900 nm/970 nm (Penuelas et al., 1995) and 1075 nm/1175 nm (Curren 1989).

These vegetation indices were used in combination with LiDAR-derived canopy height models and slope models to discriminate terrain and vegetation related SAR targets from those generated by metal objects on the terrain surface. The results of this discrimination processing are described in the Final SAR Report.

4. PERFORMANCE ASSESSMENT

4.1. Performance Objectives

Primary performance criteria included the quantitative assessment of the ease of technology usage and the quality assessment of positional accuracy and resolution. Secondary performance objectives considered the contribution of HSI to the WAA efforts, including the detection of surface metal, SAR false alarm reduction through vegetation modeling, and the probability of detection of target features and other large MRFs. These performance objectives and their descriptions are provided in Table 4.

Table 4. Performance Criteria

Performance Criteria	Description	Primary or Secondary
Technology usage	Ease and efficiency of operation	Primary
Geo-referenced position accuracy	Comparison of datasets with ortho-imagery of known accuracy	Primary
Spatial resolution	Delivered image resolution after geo-referencing	Primary
Spectral resolution	Delivered spectral resolution	Primary
Surface metal detection	Surface Metal Objects > 1500gm	Secondary
SAR false alarm reduction	Reduction in SAR false alarms related to SAR-responsive (water containing) vegetation	Secondary
Probability of Detection of target features and other large MRFs	Percent of total large munitions related features detected by analysis of HSI datasets	Secondary

4.2. Performance Confirmation Methods

Performance confirmation methods and actual post demo results are provided in Table 5. A detailed description of the analysis, interpretation, and evaluation for each performance criterion is provided in Section 4.3.

Table 5. Expected Performance and Confirmation Methods

Performance Criteria	Expected Performance Metric (pre demo)	Performance Confirmation Method	Actual (post demo)
Technology usage	Easy and efficient to use	Evaluation of availability of sensor, and timely completion of data collection and primary processing	Easy and efficient to use
Geo-referenced position accuracy	3-4.5m RMSE	Comparison of datasets with ortho-imagery of known accuracy	4.9–11.8 m RMSE
Spatial resolution	Phase I: 1.5 and 3 m Phase II: 1.5 m	Direct examination of the delivered datasets following geo-referencing using supplied geographic lookup table (GLT) files	Phase I: 1.5 and 3 m; Phase II: 1.5 m
Spectral resolution	126 bands (0.45 μm – 2.5 μm	Direct examination of the delivered datasets following geo-referencing using supplied GLT files	126 bands (0.45 μm – 2.5 μm
Surface metal detection	Detection of surface metal objects > 1500gm = 0.8	Percentage of metal features extracted from ground calibration and validation datasets detected in HSI	Surface metal detection not achievable at site
SAR false alarm reduction	Reduction in SAR false alarms	Receiver operating characteristic (ROC) evaluation of false alarm rate	Achieved
Probability of detection of target features and other large MRFs	>.90	Percentage of total large-feature MRS sites identified in other ground and WAA sensor datasets	0.46

4.3. Data Analysis, Interpretation and Evaluation

4.3.1. Technology Usage

Scheduling of the HSI data collection required coordination with other HyVista projects but no deployment problems were encountered. Furthermore, the survey of thousands of acres per day presents an efficient data collection methodology. No problems were encountered with primary processing. Calibration analysis and surface metal detection capabilities required additional field studies for assessment.

4.3.2. Geo-referenced Position Accuracy

All 21 Phase I and Phase II flight strips were geo-corrected in ENVI using the supplied GLT tables and checked for spatial registration with the orthophotography prior to use for large feature detection and analysis. Using spatial correlation with plant groupings and other features observed in the orthophotography, datasets from all flight strips were estimated to have horizontal offsets of 3-15 m, which was considered adequate registration for the large-target feature extraction processing. Spatial accuracy of the GLT-transformed HSI imagery was formally evaluated in a subset of the 21 flight strips by locating the positions of ground fiducial markers in the geo-corrected HSI imagery, then computing the X- and Y-offsets from the known GPS location of each marker.

Table 6 shows the three flight strips whose imagery was formally evaluated using fiducial marker locations and precisely calculated offsets. While the GLT-processed spatial error was adequate for large-feature detection and characterization, the radial RMSE should be less than 1 m in order for the data to be useful for detecting small metal objects or for fusion processing with SAR, LiDAR, and orthophotography data. In general, the horizontal spatial error was determined to be larger than the HyVista specification of 3m RMSE for these three flight strips, ranging from 7m in the best case, to more than 15m in the worst case.

Table 6. Horizontal Accuracy of Selected GLT-Geo-corrected HSI Flight Strips

Accuracy Metric	FL4 (m)	FL5 (m)	FL6 (m)
Y RMSE	11.71	3.00	1.09
Y Linear Error (95%)	22.94	5.89	2.14
X RMSE	0.99	7.64	4.73
X Linear Error (95%)	1.94	14.96	9.27
RMSE Horizontal Radial Error (68.3% confidence level)	11.75	8.20	4.85
Horizontal Radial Error (95% confidence level)	15.54	13.02	7.12

Table 7 shows the residual RMSE error of the polynomial warp referencing of tiled multi-strip mosaiced HSI data to the orthophotography. The process used a 4th order polynomial warp and a minimum of 60 registration control points per tile. Tiled 1.5 cell HSI band stacks were registered to the orthophotography using ground features of decreasing size identified as individual contrasting cactus plants and shrubs in the 14 cm orthophotography. Small object position in the 1.5 m resolution HSI imagery could be estimated according to whether the object was entirely within or bordering the HSI pixel. Because the initial HSI GLT correction had been generated using high resolution LiDAR terrain data, remaining geo-correction errors were well corrected by the high-order polynomial warp algorithm to less than 0.33 pixel (0.50 m).

Table 7. Horizontal Accuracy of Orthophoto-registered HSI Image tiles

Processing Tile	Residual Error 1.5 m (RMSE meters)
Tile 1	0.43
Tile 5	0.37
Tile 8	0.41

Tiles 5 and 8 contained the main bombing target zones and SAR field calibration areas, and were processed first for coregistration and spectral sharpening to support SAR signal discrimination efforts. Although the HSI/LiDAR/orthophotography fusion methodology successfully mapped a high proportion of false-alarm generators in the SAR datasets, the operating characteristics of the SAR sensor and related target extraction processing limited surface metal detection to relatively large objects that were not representative of *in situ* metal on the site. Therefore, the other 6 tiles were not processed to the higher resolution and spatial accuracy.

4.3.3. Spatial and Spectral Resolution

Spatial resolution of the basic hyperspectral datasets delivered by HyVista met the specifications of 1.5 and 3 m resolution for the Phase I datasets, and 1.5 m for the Phase II datasets. As described below, the principal components spectral sharpening algorithm used to increase spatial resolution through fusion with the RED orthophoto image band successfully increased the HSI image resolution to 0.25 m while maintaining adequate spectral resolution to detect concentrations of succulent vegetation on the landscape surface for SAR signal discrimination. However, increased noise in the sharpened imagery did not allow detection of subtle shifts in iron absorption features necessary to spatially correlate spectral features with metal object locations on the ground.

4.3.4. Surface Metal Detection

The calibration studies described in Section 3 did not succeed in using HSI data to directly detect sub-pixel sized metal features on the landscape surface. Consequently, the surface metal detection objective of the demonstration was concluded with no further site-wide analysis.

While an attempt was made to execute this discrimination by associating clay and carbonate-related absorption features (aluminum/carbonate) with lithological iron oxide, presupposing that iron oxides not associated with clay and carbonate might be munitions-related iron, this strategy was defeated in the calibration tests by several factors. Primarily, the abundance of lithological iron visible to the sensor was enhanced by the proportion of exposed bare mineral soil not covered by vegetation, and the likelihood that a 1.5 m or 3 m pixel containing metal fragments would contain dominant amounts of bare mineral soil compared to iron-oxide coated metal. Other factors contributing to the inability of the calibration analysis to discriminate metal objects included the relatively poor spatial geo-referenced positioning of the basic GLT-corrected data, making it difficult to determine the data pixel containing a particular field-located object, and the basic size of the type of metal objects present at the site in comparison to the image pixel size. As described above, when the data were re-sampled to perform a tight registration with the orthophotography, the spectral quality of the data was reduced so that very subtle absorption feature shifts could not be detected with confidence. Therefore, the demonstration did not generate significant direct detection of munitions-related metal objects at the site.

The inability to attain this demonstration objective should not be construed as an indication that airborne imaging spectrometers cannot be used for direct WAA detection of munitions-related materials at UXO response sites. Site phenomenology plays a significant role, and better spectral contrast between materials of interest and natural landscape materials is possible at sites with larger metal objects and/or different soil chemistry. Additionally, HSI sensors are under continuing development to increase spectral and spatial resolution, with increasing capability to "tune" the spectral response capabilities for specific materials detection tasks. One significant prospect is the direct detection of munitions-related chemical residues in the soil such as phosphorus, napalm, mercury, TNT, and ammonium nitrate. Indeed, the success in detecting terrain-obscured ship outline targets described in the previous section may be related to the detection of paint or marker residues in the soil associated with marking the target outlines on the ground. Therefore, the results of surface metal calibration study are a valuable guide to future efforts for direct surface metal detection using HSI.

4.3.5. SAR False Alarm Reduction

As described in the Final SAR Report, the ability to effectively detect metal objects with the SAR sensor at the Pueblo site required the individual identification of water-bearing plant species such as cactus and yucca so that SAR target signals associated with these plants could be filtered from the population of SAR object detections. Figure 13 shows an example of vegetation indices derived from the sharpened and spatially registered HSI data, together with the orthophoto, LiDAR canopy height model, and SAR image for a region approximately 20 m x 20 m centered on a group of 5 yucca plants. These images illustrate the spatial registration of plant material detections in the HSI to indicators in the orthophoto and to SAR signals

Although the detection of small metal objects by SAR had significant issues related to the capability to separate small metal objects from background noise, metal objects of sufficient size were effectively discriminated from vegetation objects using the HSI-derived data, as illustrated in Figure 14. The ROC curves in Figure 14 illustrate that for detection of metal objects with SAR response similar in magnitude to vegetation–generated targets, the HSI-derived vegetation discrimination masks achieve a reduction in false alarms. At the Pueblo Simulated Ordnance (SimOrd) calibration site, false alarm generators were nearly an order of magnitude more abundant than metal targets, so reducing the false alarm rate to less than the number of real targets (21) was considered to be the key to detecting density concentrations of metal targets. Figure 14 illustrates a shift in the ROC curve for each discrimination factor relative to the "SAR Only" curve. The "Combined" discrimination method ROC curve shows a reduction of false alarms to 12, with a detection rate greater than 0.5 at the most selective SAR amplitude threshold, while the detection rate of the "SAR Only" curve is 0.8 and includes more than 50 false alarms. In an environment where the targets can be detected with a false alarm rate at or below the detection rate, it should be possible to detect target density clusters, but for false alarm rates much higher than detection rates, density analysis is unlikely to be meaningful.

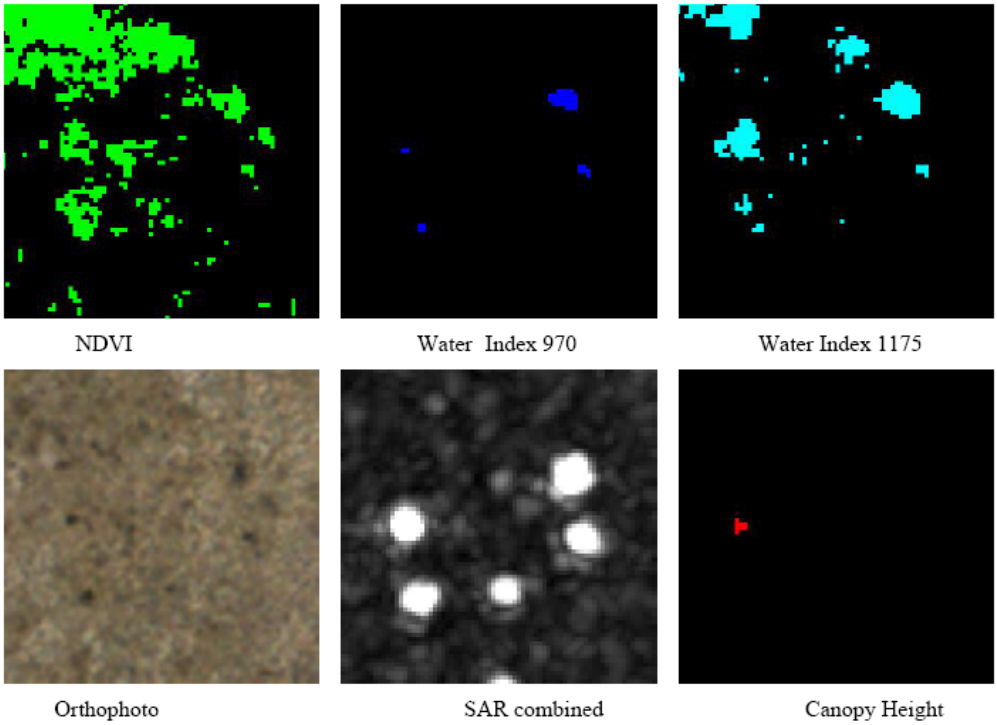

Figure 13. Top Row: Vegetation indices derived from HSI data. Bottom Row: Ortho, SAR and LiDAR data from same area. (Image Chip: 40 m X 40 m, 25 cm pixels. Normalized Difference Vegetation Index (NDVI) is calculated as [NIR – RED]/[NIR + RED] and the Water Indices are simple ratios of reflectance within key water absorption spectral ranges relative to adjacent spectral ranges.)

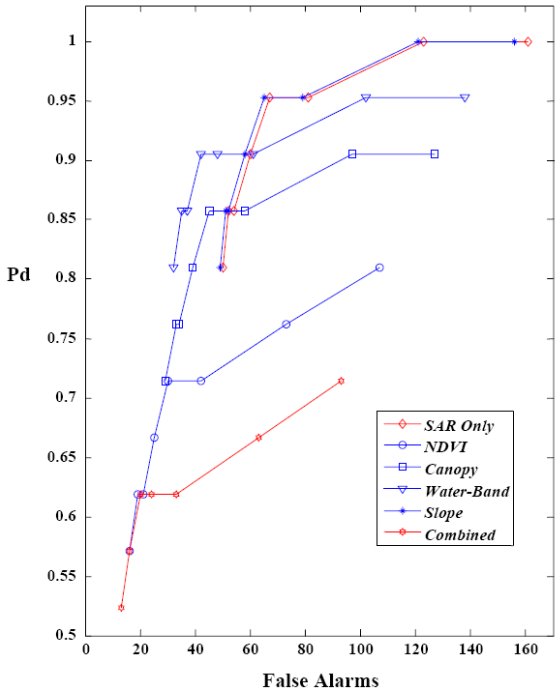

Figure 14. ROC curves for metal targets in the SimOrd calibration area illustrating false alarms and the probability of detection for 21 simulated ordnance targets at various SAR signal amplitude thresholds and using HSI-derived vegetation discrimination masks singly and in combination.

4.3.6. Probability of Detection of Target Features and Other Large MRFs

The strategy of using HSI imagery to detect and map large munitions-related features such as target circles and disturbed ground areas proved to be a useful adjunct to the LiDAR and large scale orthophotography datasets, but because of reduced spatial resolution and accuracy, would not be a successful substitute for either.

However, for 2 of the 4 ship targets observed in the vicinity of BT4 the HSI data actually contributed significantly to the detection and confirmation of these targets, which were topographically obscured in the LiDAR data and very difficult to detect in the orthophotography data. Therefore, the summary in Table 8 indicating a good detection rate for ship targets and a relatively low detection rate for smaller disturbance features is somewhat misleading concerning the demonstrated value of HSI large-feature detection to the overall WAA process. In fact, as illustrated in Figures 11 and 12, the use of HSI imagery with advanced processing techniques significantly improved the detectability of many of the large features on the site.

Table 8. Large Feature Detection Comparison

Feature Type	Observed in HSI	Total Observed	Percent Detection
Target Circles	3	4	0.75
Target Crosses	0	4	0.00
Ship Targets	4	4	1.00
Other Significant Features	3	10	0.33
Total Large Features	10	22	0.46

This detection capability successfully used image visualizations generated by sophisticated image processing techniques that reduced the 126-band HSI image cube down to a dozen or so information-rich synthetic spectral bands using a noise-filtering principal components rotation process. This approach can be generalized to assist WAA feature detection processes under a wide range of site types and landscape conditions wherever HSI datasets are available.

4.3.7. Performance Assessment Summary

Airborne imaging spectrometers such as the HyVista HSI demonstrated for this project as a part of the WAA Pilot Program can be used in a variety of ways to augment the high airborne portion of the WAA data collection process. Although the HSI sensor alone would not out-perform the LiDAR/Orthophotography sensor combination in general site characterization, and did not meet expected performance criteria in several areas, this demonstration showed that HSI imagery can be effectively used to detect and extract large munitions-related features such as target aiming features and landscape disturbance patterns. The demonstration also successfully showed how HSI datasets can be used in a multiple-sensor fusion process to perform false-alarm reduction for synthetic aperture radar object detection protocols. For direct detection of metallic objects such as UXO and munitions scrap, the demonstration generated useful information concerning the spatial and spectral resolution requirements, and detection phenomenology parameters necessary to make direct detection using airborne spectrometers useful in a WAA scenario.

5. COST ASSESSMENT

5.1. Cost Reporting

Cost information associated with the demonstration of all airborne technology, as well as associated activities, were tracked and documented before, during, and after the demonstration to provide a basis for determination of the operational costs associated with this technology. For this demonstration, Table 9 contains the cost elements that were tracked and documented for this demonstration. These costs include both operational and capital costs associated with system design and construction; salary and travel costs for support staff; subcontract costs associated with airborne services, support personnel, and leased equipment; and costs associated with the processing, analysis, comparison, and interpretation of airborne results generated by this demonstration.

Table 9. Cost Tracking

COST CATEGORY	SUB CATEGORY	DETAILS	COSTS ($)
START-UP COSTS	Pre-Deployment and Planning	Includes planning, contracting, site visit and site inspection	$30,481
	Mobilization	Personnel mobilization, equipment mobilization, transportation, site preparation and fiducial marker emplacement	$15,240
OPERATING COSTS	Data collection and processing costs	HSI data acquisition and associated tasks; and data processing	$95,728
DEMOBILIZATION	Demobilization	Demobilization, packing, fiducial marker removal	$15,240
ANALYSIS	Analysis of HSI datasets	Analysis, feature detection, vegetation modeling and data fusion	$46,261
MANAGEMENT	Management and Reporting	Project related management, reporting and contracting	$66,114
TOTAL COSTS			
		Total Technology Cost	$269,065
		Acres Surveyed	9,754
		Unit Cost	$28/acre

5.2. Cost Analysis

The major cost item for an airborne survey system is the cost of aircraft airtime.. Data processing and analysis functions made up the bulk of the remaining costs.

The costs associated with field calibration and analysis of the ability of HSI to detect surface metal and the vegetation modeling for SAR false alarm reduction were major factors in this particular survey. Costs for HSI surveys not incorporating vegetation modeling would be expected to be less. In addition, if surface metal detection is a survey objective, pre-analysis of a site to determine if the detection of surface metal is feasible given site specific conditions is recommended before undertaking an airborne survey.

Project management and reporting were a significant cost for this demonstration, as the project was conducted under the WAA Pilot Program and required more meetings, travel, and reporting than would generally be expected for a production-level survey. Last, mobilization and demobilization can be a significant task in terms of cost. Generally, this is a function of distance from the home base for the aircraft, equipment and personnel.

Costs associated with validation were not considered in the cost analysis, as the validation was conducted as part of the Wide Area Assessment Pilot Program.

6. IMPLEMENTATION ISSUES

6.1. Regulatory and End-User Issues

The ESTCP Program Office has established a Wide Area Assessment Pilot Program Advisory Group to facilitate interactions with the regulatory community and potential end-users of this technology. Members of the Advisory Group include representatives of the US Environmental Protection Agency, State regulators, US Army Corps of Engineers officials, and representatives from the services. ESTCP staff has worked with the Advisory Group to define goals for the Pilot Program and develop Project Quality Objectives. As the analyzed data from the demonstrations become available, the Advisory Group will assist in developing a validation plan.

There will be a number of issues to be overcome to allow implementation of WAA beyond the pilot program. Most central is the change in mindset that will be required if the goals of WAA extend from delineating target areas to collecting data that is useful in making decisions about areas where there is not indication of munitions use. A main challenge of the pilot program is to collect sufficient data and perform sufficient evaluation that the applicability of these technologies to uncontaminated land and their limitations are well understood and documents. Similarly, demonstrating that WAA data can be used to provide information on target areas regarding boundaries, density and types of munitions to be used for prioritization, cost estimation and planning will require that the error and uncertainties in these parameters are well documented in the program.

7. REFERENCES

Curren P. J., 1989, Remote Sensing of Foliar Chemistry. Remote Sensing of Environment, 30, 271–278.

Penuelas, J., I. Filella, C. Biel, L. Serrano, and R. Save, 1995. The Reflectance at the 950-970 Region as an Indicator of Plant Water Status. International Journal of Remote Sensing 14:1887-1905.

Pulsipher, B., Hathaway, J., McKinstry, C., McKenna, S., and B. Roberts, "Transect Design and Target Area Identification Approach for the Pueblo Precision Bombing range and Pattern Gunnery Range #2 WAA Site," *in* Proceedings Partners in Environmental Technology Technical Symposium & Workshop, Washington DC, November 2005.

Sellers, P.J., 1985. Canopy Reflectance, Photosynthesis and Transpiration. International Journal of Remote Sensing 6:1335-1372

Versar, Inc., "Conceptual Site Model to Support ESTCP Wide Area Assessment Program" Draft ESTCP Version 0 Report, June 2005.

Vrabel, J., Doraiswamy, P., McMurtrey, J., and Stern, A (2002). "Demonstration of the Accuracy of Improved Resolution Hyperspectral Imagery", SPIE Symposium Proceedings.

Welch, R. and W. Ahlers, 1987. "Merging Multiresolution SPOT HRV and Landsat TM Data." Photogrammetric Engineering & Remote Sensing, 53 (3), pp. 301-303

8. POINTS OF CONTACT

Table 10. Points of Contact

POINT OF CONTACT Name	ORGANIZATION Name Address	Phone/Fax	Role in Project
Dr. John Foley	Sky Research, Inc. 445 Dead Indian Road Ashland, OR 97520	(Tel) 978.479.9519 (Fax) 720.293.9666	Principal Investigator
Sky	Sky Research, Inc. 445 Dead Indian Road Ashland, OR 97520	(Tel) 541.552.5102 (Fax) 541.488.4606	Co-Principal Investigator
Mr. Jerry Hodgson	USACE Omaha District 215 N. 17th Street Omaha, NE 68102-4978	(Tel) 402.221.7709 (Fax) 402.221.7838	Federal Advocate
Mr. Hollis (Jay) Bennett	US Army R&D Center (CEERD-EE-C) 3909 Halls Ferry Road Vicksburg, MS 39180-6199	(Tel) 601.634.3924	DoD Service Liaison